Pergamon

Int. J. Multiphase Flow Vol. 23, No. 2, pp. 227–247, 1997

0301-9322/97 $17.00 + 0.00

PII: S0301-9322(96)00075-4

SIMILARITY LAW AND TURBULENCE INTENSITY PROFILES IN A BUBBLY BOUNDARY LAYER AT LOW VOID FRACTIONS

J. L. MARIÉ, E. MOURSALI and S. TRAN-CONG

Laboratoire de Mécanique des Fluides et d'Acoustique, UMR C.N.R.S. 5509,
Ecole Centrale de Lyon/Université Claude Bernard Lyon I ECL, BP 163, 69131 Ecully Cedex, France

(Received 26 October 1995; in revised form 1 October 1996)

Abstract—This paper follows on from the research recently published by Moursali *et al.* (1995a). While the first data reported were relative to the void migration, the wall shear stress and in a very limited extent to the liquid velocity, the present results provide new information on the kinematic and turbulent structure of a bubbly boundary layer at low air concentrations. The mean liquid velocity is shown experimentally to obey a modified logarithmic law of the wall in the presence of millimetric bubbles. An expression for this modified law is derived by simple analytical considerations and non-dimensional scaling. The skin friction calculated on this theoretical basis fits the measurements satisfactorily. Longitudinal turbulence intensity profiles are also obtained. They show that the turbulence is increased by two relatively uncoupled mechanisms: a modification of the wall production and the creation of pseudo-turbulence in the external layer. Finally, the mixing length inferred from the data is given and compared with some of the models which are proposed in the literature. © 1997 Elsevier Science Ltd. All rights reserved.

Key Words: bubbly boundary layer, modified law of the wall, turbulence intensity, mixing length

1. INTRODUCTION

The detailed description of the wall region in a bubbly flow is of real interest for specifying the boundary conditions close to the surface to be implemented in numerical codes (Lance and Lopez de Bertodano 1992). Referring to the literature, the structure of upward wall-bounded bubbly flows has generally been analysed for pipe geometries (Serizawa *et al.* 1975; Sato *et al.* 1981; Nakoryakov *et al.* 1981; Wang *et al.* 1987; Souhar 1989, Liu 1993) and is well documented. However, the small diameter of the pipes makes the investigation of the flow close to the surface quite difficult when using the standard local probes or almost impossible by means of high speed camera visualization technique.

The study of another-wall bounded flow pattern is therefore useful, provided that the aforementioned difficulties are not encountered. The authors have selected the case of a turbulent boundary layer developing on a vertical flat plate in the presence of millimetric bubbles, both because of its much simpler geometry and of its practical advantages. Of course the choice of a different configuration may lead to significant differences in the observations, but it is expected that the basic mechanisms involved in the two situations—pipe or flat plate—will remain, for the most part, very similar.

The first results of this research which recently appeared in Moursali *et al.* (1995a) support this idea. They mainly concern the question of phase distribution. The void fraction profiles obtained in the section $x = 1$ m downstream of the leading edge, exhibit a sharp relative or absolute maximum, ϵ_P, at a distance of the order of the mean equivalent radius of the bubbles from the wall and asymptotically recover their free-stream value. The void peaking phenomenon observed here close to the plate is consistent with the findings of a number of authors dealing with upward pipe flow (Serizawa *et al.* 1975). By taking high speed video films of the flow it was shown that this phenomenon could be attributed to a deceleration of the bubbles at the surface and to a significant number or bubbles which were deflected towards the wall. These so called migrations seem to be quite random and characterized by a short timescale. As noted in Moursali *et al.* (1995b), the frequency of the void migration proves to scale quite nicely when using the typical

time scale of the single-phase bursting process, suggesting that the motion of the migrating bubbles might be the result of their interaction with some coherent structures. Moreover, it is mainly the small bubbles ($\bar{D}_B \approx 3.5$ mm) which migrate and remain at the wall, whereas the large ones concentrate in the outer stream. Similar conclusions have been reached by Serizawa *et al.* (1988), Monji and Matsui (1991), Liu (1993), Zun *et al.* (1992). An investigation in progress in our laboratory has provided extra information on this question (Tran-Cong *et al.* 1996), in the case where a few number of bubbles, with a given size, were released near the plate from a single nozzle. Concerning the skin fraction, our measurements indicate that the shear stress at the wall is increased by the presence of the bubbles. This is also in agreement with all the data of the pipe literature with the same range of parameters (bubble size, void fraction, flow direction, liquid velocity).

The influence of the void peaking distribution on the mean liquid velocity and longitudinal turbulent intensity profiles is analysed in the current work. The experimental facility, operating conditions and measuring techniques are described in sections 2 and 3. In section 4.1, the modifications of the velocity profiles are discussed. In particular it is shown that the standard kinematic structure of the initial turbulent boundary layer is preserved with, however, a modified law of the wall. Based on simple theoretical arguments, an expression for this new law is derived in section 4.2 and tested in its ability to predict the increase of wall shear stress, for which measurements are available (Moursali *et al.* 1995a). The possibility of extending these results to bubbly flows in pipes is examined section 4.3, in the light of the available data and of the previous model (1987a). Section 5.1 is devoted to the experimental study of the action of the bubbles on the turbulence production. Surprisingly, the longitudinal turbulence intensity is slightly modified in the intermediate layer (logarithmic zone), although it increases significantly outside by two distinct mechanisms: an extra wall production caused by a higher mean liquid velocity gradient and a generation of pseudo-turbulence in the outer region. Finally, in section 5.2 it is shown that the use of a mixing length is justified at low void fraction and that the model inferred from our data compares quite well with certain expressions recommended in the literature.

2. EXPERIMENTAL FACILITY: DESCRIPTION AND OPERATING CHARACTERISTICS

A detailed description of the facility is given in Lance and Bataille (1991) and Moursali *et al.* (1995a). The sketch of the experiment (see the second reference) is displayed in figure 1. The flat plate is located at the centre of the test section of a vertical water tunnel. The latter is operated in the upward direction at atmospheric pressure, ambient temperature and at liquid velocities which do not exceed 1.5 m/s. The water was filtered and decalcified, but no other precaution was taken to remove impurities in view of the dimensions of the facility. Under such conditions it is expected that the water is contaminated. Air is blown uniformly into the liquid upstream of the inlet of the test section by means of an array of needles fixed on a square mesh grid. The void fraction obtained with this kind of injector varies from 0 to 6% depending on the injection pressure. The plate, which is 15 mm thick, 400 mm wide (z-direction), and 2 m long (x-direction) is made of plexiglass. Its ogive shaped leading edge lies 0.5 m downstream of the entrance. The transition of the boundary layer is triggered by a rough abrasive ribbon, 3 cm wide, stuck on the surface immediately downstream of the leading edge.

LDA measurements made in the absence of bubbles showed that the turbulent boundary layer had a standard structure (Schlichting 1968). In particular there is no significant pressure gradient along the x-axis, and the low free-stream turbulence ($<1\%$) generated by the injection grid does not affect the flow on the plate (Hancock and Bradshaw 1983). For an external velocity, U_E, of 1 m/s, the thickness, δ, of the boundary layer is of the order of 22 mm at the station $x = 1$ m, and the associated Reynolds number, R_δ, is of the order of 22,000. Regarding the inlet conditions, the liquid and void fraction profiles upstream of the flat plate prove to be quite flat, as required. The granulometry of the bubbles was determined by using two complementary techniques: an optical probe and a high speed video camera (section 3). Two distinct regimes of injection were observed (figure 2, Moursali *et al.* 1995a). At very low void fractions ($0\% < \epsilon < 1.5\%$), the bubbles are small, quite uniform in size, with a mean equivalent diameter $\bar{D}_B = 3.5$ mm, whereas at higher void fractions ($3\% < \epsilon < 5.5\%$), the equivalent diameters of the bubbles range from 3 to 8 mm, most of them being closer to 6 mm. Over that range, the bubbles are approximately oblate spheroidal,

and have a mean velocity, U_B, given by: $U_B = U_L + U_R$, where the relative velocity, U_R, is of the order of 20 cm/s.

The results reported hereafter were obtained at station $x = 1$ m downstream of the leading edge, under the first injection regime. As mentioned above, this corresponds to the case where the bubbles are small (of order of 3 mm) and for which migration takes place. The associated void fraction profiles are typically of the form exhibited in figure 3. They are characterized by a sharp maximum at the wall, ϵ_P (which roughly extends to a distance of the order of the mean bubble diameter from the wall), and a large flat shape portion at constant free-stream value, ϵ_E. The variation of ϵ_P as a function of ϵ_E and of the associated bubble number per unit of time: F_E, F_P, is given in table 1 for the range of void fraction considered.

3. INSTRUMENTATION

All intrusive probes were fixed on a rod whose motion in the transverse direction was controlled by a motorized micrometer screw device. Their initial distance from the wall was adjusted using a telescope. The zero was taken as the probes came into contact with the plate. An optical transducer was used to read their exact position with an accuracy of 10 μm. The local bubble frequency and the void fraction, ϵ, were determined using an Optoflow 'Photonectics' optical probe whose measuring volume is of the order of $(50\ \mu m)^3$. The rise velocities, shapes and trajectories of individual bubbles were estimated from high speed video films taken with a NAC-VHS camera (200 frames/s). The friction velocity, U^*, was inferred from measurements of the two-phase local

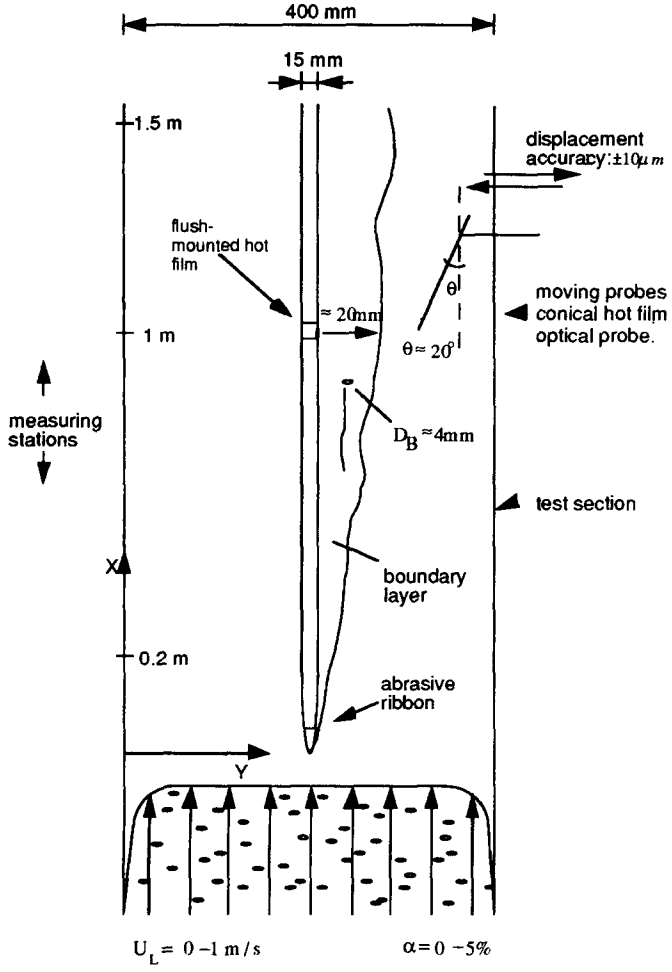

Figure 1. Sketch of the experiment (Moursali *et al.* 1995).

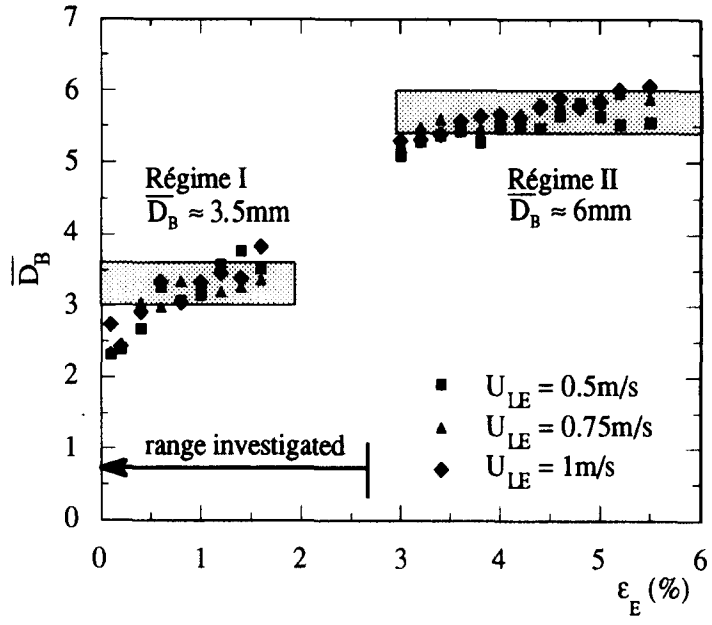

Figure 2. Mean equivalent diameter of the bubbles upstream of the plate (Moursali *et al.* 1995).

wall shear stress, made with a flush-mounted hot film. For further details about these various measuring techniques as well as the signal processing procedure, the reader should refer to Moursali *et al.* (1995a).

The mean liquid velocity and longitudinal turbulent intensity profiles, $U_L(y)$ and $u'_L(y)$, were measured by means of a miniature TSI 1264 AW-BR conical hot film connected to a TSI IFA100 constant temperature anemometer. It was preferred to a Laser Doppler anemometer, because the use of the latter is particularly delicate with millimetric bubbles (Marié 1983; Cartellier and Achard 1985) and soon limited as the void fraction increases (Marié and Lance 1983), which is typically the case close to the wall. The conical rather than the cylindrical shape was chosen, because it is less sensitive to impurities and because the piercing of the bubbles is sharper, especially close to the wall. Since its apex angle is 40°, the probe was inclined at an angle of 20° from the flow (or

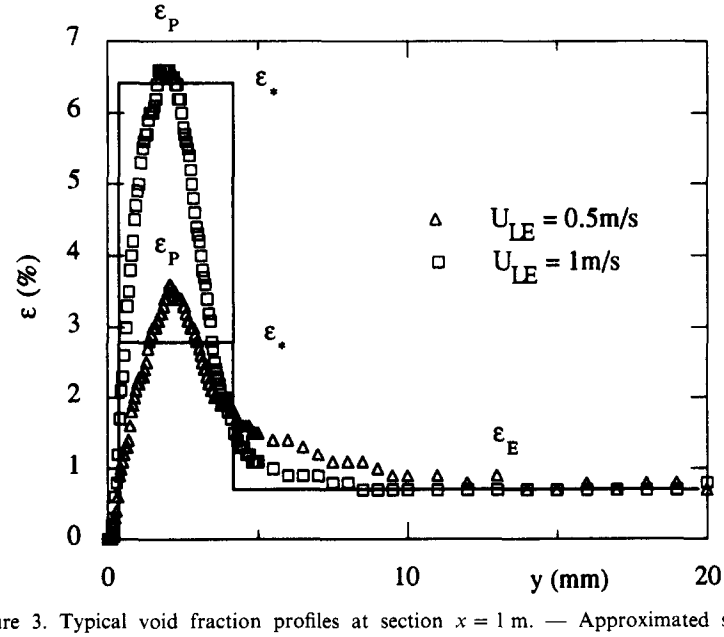

Figure 3. Typical void fraction profiles at section $x = 1$ m. — Approximated shape.

Table 1. Parameters for the scaling of the wall layer

U_{LE} (m/s)	ϵ_E (%)	F_E (/s)	ϵ_P (%)	F_P (/s)	U_*' (m/s)	K'	C'	U_*^* (m/s)	C^*
0.75	0.0	0.00	0.0	0.00	0.034	0.41	4.9	0.034	4.9
0.75	0.2	1.71	2.0	4.72	0.037	0.53	6.2	0.028	8.6
0.75	0.5	3.40	3.5	8.75	0.039	0.62	6.8	0.026	12.4
0.75	1.5	9.25	6.0	17.24	0.044	0.78	7.6	0.025	15.8
1.0	0.0	0.00	0.0	0.00	0.045	0.41	4.9	0.045	4.9
1.0	0.2	2.14	1.6	6.23	0.047	0.45	5.5	0.042	6.4
1.0	0.5	4.12	3.8	11.97	0.049	0.53	6.1	0.037	8.4
1.0	1.5	10.80	6.8	21.50	0.052	0.65	7.0	0.037	12.3

plate direction) in order to reach the surface. In the free-stream, the angular response of the probe was found to be relatively insensitive to its inclination with respect to the flow up to $\pm 20°$ (see figure 4(a)). In what follows, it is assumed that such a behaviour still holds inside the boundary layer. In the immediate vicinity of the wall, however, the diameter of the sensitive ring of the probe is of the order of the thickness of the viscous sublayer (0.1 mm), i.e. of the order of a typical length scale over which the velocity varies significantly. As a consequence, the measurements made in that region are expected to be inaccurate. Indeed in single-phase flow, at a given station $x = 1$ m and free-stream velocity $U_E = 1$ m/s, the longitudinal turbulent intensity profile only proved to be in good agreement with that given by Klebanoff (1955) and others, if the maximum of both curves were made to coincide, i.e. if a very small shift of the origin of the y coordinate was performed ($y_0 = 50\ \mu$m). This of course means that when the probe was touching the wall, the turbulent intensity actually measured was that prevailing at a distance $y_0 = 50\ \mu$m from the wall. This shift of the origin was taken to be the same in the presence of bubbles. This assumption, which might very well be questioned, is immaterial in the present context since y_0 is quite small compared to the range of y of interest. The signal delivered by the anemometer was analogous to that observed in other experiments reported in the literature (Wang *et al.* 1987) and was processed using a thresholding technique applied to its time derivative, as discussed in Lance and Bataille (1991), Moursali (1993) and schematically illustrated in figure 4(b). Close to the wall however, ($y^+ \leqslant 20$), an additional difficulty arises from the above procedure since the amplitude of some of the high frequency components of the liquid velocity fluctuation become of the same order of magnitude as that of the peaks associated with the piercing of bubbles. In order to make up for the associated loss of information concerning the liquid, when determining its characteristic function $\chi_L(t)$, the acquisition time was significantly increased. The error of such measurements is maximum close to the plate, where conduction problems take place at the surface and where the spatial resolution of the probe is bad, compared with the inhomogeneity scale. As seen in figure 6 ($\epsilon_P = 0\%$), the uncertainty for single-phase runs, is of the order of 30–50% in the viscous sublayer, but it does not exceed 10% in the other parts of the flow. Roughly the same accuracy is expected with bubbles.

4. KINEMATIC STRUCTURE

4.1. Mean liquid velocity profiles

The influence of migration on the characteristics of the boundary layer was first analysed through the modifications of the local mean liquid velocities. The latter were measured at various external void fractions, ϵ_E, up to 1.5% (first injection regime in figure 2), keeping the mean liquid velocity in the free-stream, U_{LE}, constant. It must be stressed that the measurements in the pipe literature are usually performed at a given superficial liquid velocity. Here, the choice of other flow conditions was made with, as a first step, the intention of disregarding the acceleration effects generated by the bubbles in the outer region. Typical profiles at station $x = 1$ m are shown in figure 5. In the immediate vicinity of the plate, the main effect of the bubbles is an increase of the mean liquid velocity gradient with, as a consequence, a flattening of the shape of the profile in the outer region. As far as we can judge on these data, the boundary layer thickness, δ, seems to be almost unaffected by the bubbles, however this result is more precisely confirmed by the shape of longitudinal turbulent intensity profiles (section 5.1). Additional information on the structure of the flow is obtained by plotting these profiles in dimensionless form, using the two-phase friction velocity

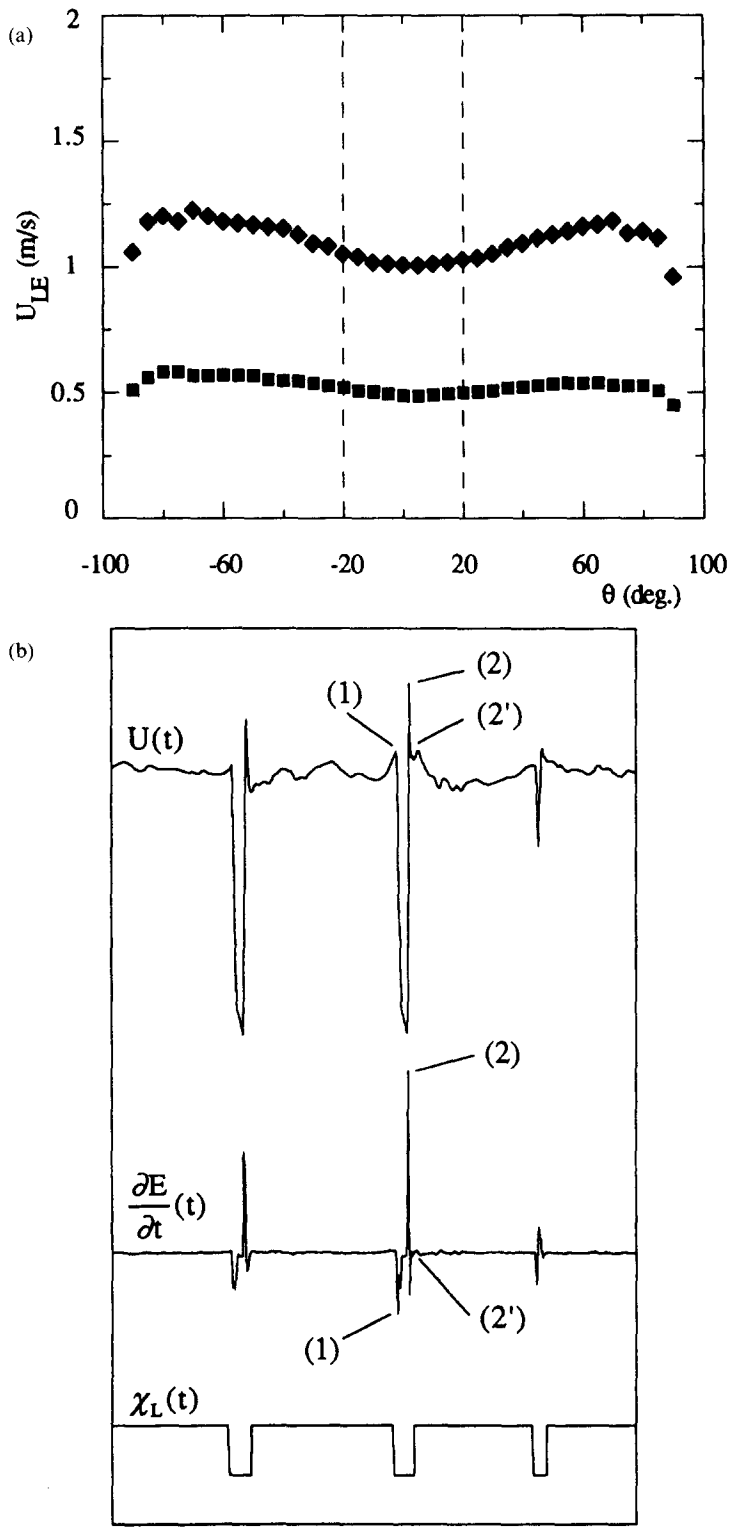

Figure 4. (a) Angular response of the miniature conical hot film TSI 1264 AW-BR. (b) Discrimination process for the conical hot film according to Moursali (1993): (1) point of the first maximum; (2') point after the second maximum (2) where the signal time derivative recovers the value typical of the liquid phase.

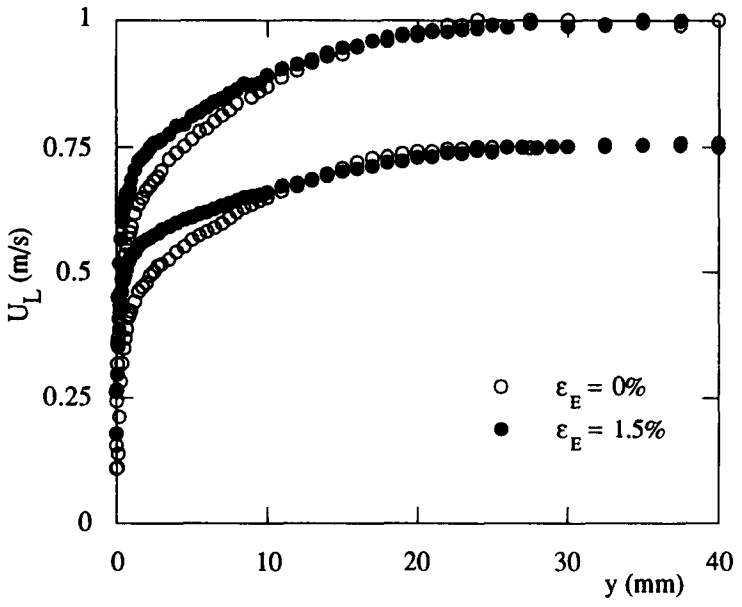

Figure 5. Mean liquid velocity profiles at station $x = 1$ m; $U_{LE} = 0.75$ and 1 m/s.

directly derived from the wall shear stress measurements (Moursali *et al.* 1995a). The logarithmic plot of the velocity in terms of the inner variable,

$$y^+ = \frac{yU_*'}{\nu},$$

shows by comparison with the single-phase wall-bounded flow theory (Tennekes and Lumley 1972), that the three zones usually encountered in a single-phase boundary layer are preserved: viscous sublayer, logarithmic zone, and the wake region (figure 6). That such a result holds might intuitively be considered as obvious in view of the low free-stream void fractions investigated here. However, one should keep in mind that in the vicinity of the wall, the peak void fraction, ϵ_P, can be as high as 7% (figure 3). In the range $y^+ = 30$–200, which corresponds to a domain where y is of the order of $\bar{D}_B$, the velocity profiles can be described by a logarithmic law, whose constants K' and C' differ from the single-phase values K and C and are functions of ϵ_E, ϵ_P, and U_{LE} (see table 1). The persistence of the logarithmic region suggests that the equilibrium production–dissipation process which is characteristic of the single-phase boundary layer still exists with bubbles. Very close to the wall, despite some scatter in the data, the non-dimensional thickness, s, of the viscous sublayer—defined here, as the ordinate of the intersection of the logarithmic and linear parts of the velocity profile (that is $s = 10.6$)—is approximately constant. Incidentally, it is a straightforward matter to derive from the latter property a value of the additive constant C' in terms of K, C, K' and s

$$C' = s\left(1 - \frac{K}{K'}\right) + \frac{K}{K'}C \qquad [1]$$

which turns out to be in good agreement with the experimental data.

Finally, in the outer region ($y^+ > 200$), the flattening of the profiles is associated with a progressive depression of the wake function as ϵ_E increases. As will be demonstrated in the next section, such behaviour results directly from the increase of K', which itself finds its origin in the gravity effects generated by the high bubble density at the surface. Furthermore, the pseudo-turbulence produced by the bubbles in the free-stream may play a significant role in the flattening process (Marié 1987a). However, in our case it remains too low for its effect to be detectable in the presence of the other prevailing mechanism.

4.2. The law of the wall

In this section, an analytical expression for the modified logarithmic law of the wall is derived from scaling considerations on the momentum equation for the liquid phase in the two-fluid model (Ishii 1975). For a stationary, fully developed upward bubbly flow in a channel (width $2h$), integration of this latter equation over a distance y from the wall (Sato and Sekoguchi 1975) leads to a relationship of the form

$$\frac{\tau}{\rho U_*^2} = \left(1 - \frac{y}{h}\right)\left(1 - \frac{gh}{U_*^2}\left[\langle\epsilon\rangle_h - \langle\epsilon\rangle_{h-y}\right]\right) \qquad [2]$$

in which $\langle\epsilon\rangle_h$ and $\langle\epsilon\rangle_{h-y}$ are the average void fractions from the surface up to the centre of the channel and from the position y up to the centre. Equation [2] is valid under the usual simplifications, that is, mainly equating the pressures in the liquid and the gas, and neglecting in the stress the terms weighted by the gas density. The same integral method plus the standard

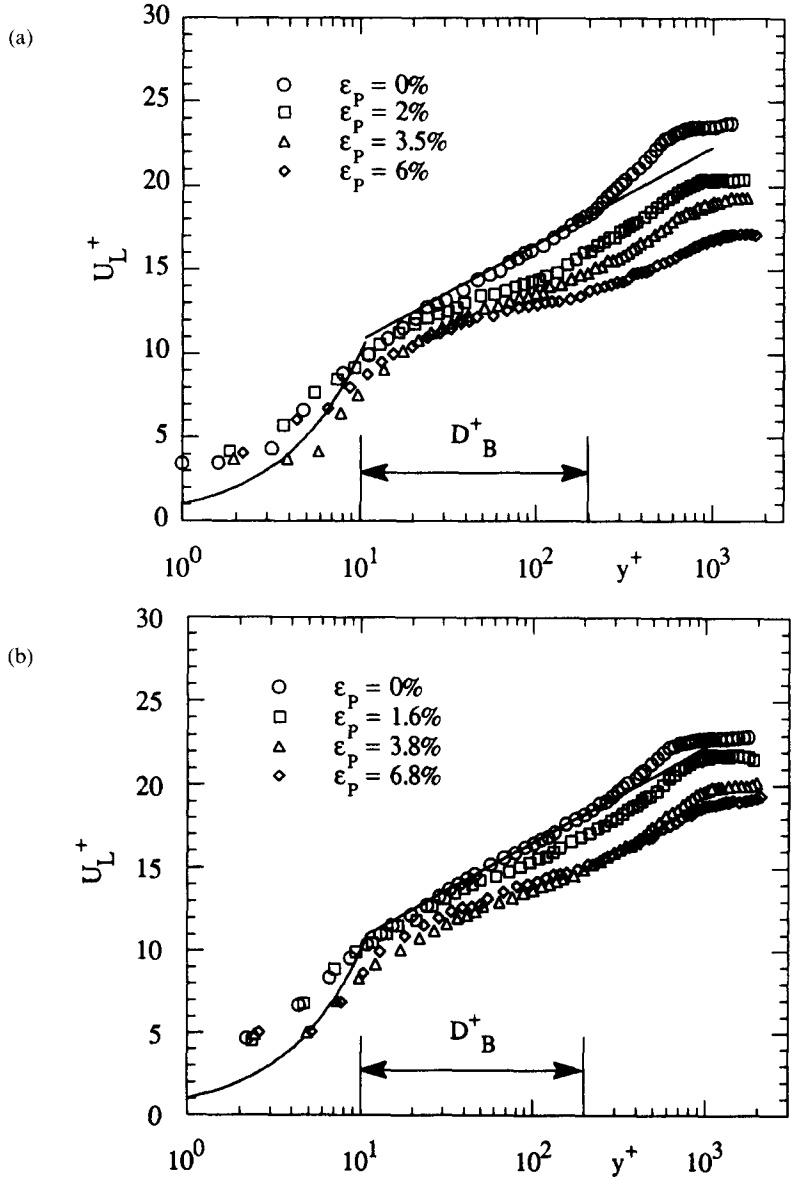

Figure 6. Velocity profiles plotted in standard inner variables. $x = 1$ m. — theory ($\epsilon_P = 0\%$). Log law: $2.5 \ln y^+ + 5$. (a) $U_{LE} = 0.75$ m/s, (b) $U_{LE} = 1$ m/s.

approximations for a turbulent boundary layer on a flat plate (Tennekes and Lumley 1972) gives, for the inner region only, the following balance

$$\frac{\tau}{\rho} = U_*'^2 - g\int_0^y (\epsilon - \epsilon_E)\mathrm{d}y. \qquad [3]$$

The order of magnitude of the term in the integral can be easily estimated. Indeed the typical shape of the void fraction profiles (figure 3) can be approximated by a rectangular step distribution with a zero value in the sublayer, a constant average peak value, ϵ_*, over the logarithmic layer and a constant free stream value, ϵ_E. Accordingly, [3] reduces to

$$(1-\epsilon)\left(\nu\frac{\partial \overline{U}_L^x}{\partial y} - \overline{u_L v_L}^x\right) = U_*'^2 - g(\epsilon_* - \epsilon_E)y \qquad [4]$$

where symbol (—x) stands for the local phase average. For the sake of simplicity, $\overline{U}_L^x$ will be denoted by U_L in what follows. In the logarithmic range, y is typically of the order of $\tilde{D}_B$ and ϵ_* roughly of the order of ϵ_P, ($\epsilon_P > \epsilon_E$). We therefore deduce that in the overlapping area

$$-\overline{u_L v_L}^x \approx U_*'^2 - g(\epsilon_* - \epsilon_E)\tilde{D}_B = U_*^{x2}. \qquad [5]$$

Such a result suggests that U_*' is no longer the velocity scale which is adapted for describing the level of shear stress in the wall region, but that the physically meaningful scaling is the new wall velocity, U_*^x, defined by [5]. This should also apply to the mean liquid velocity, hence the previous profiles have been replotted in figures 7, replacing U_*' by U_*^x. In this form, the most interesting feature is that the slope of the logarithmic law remains unchanged, while its origin is simply shifted upward, depending on the void fraction. This behaviour is even more visible on the enlarged views presented in figure 8. It is clear that the universal character of the overlapping region is preserved, provided that an appropriate logarithmic velocity scale is used. The same general conclusion has already been reported by Tennekes (1965) for turbulent boundary layers exhibiting distinct inner and outer layers, such as boundary layers with suction or injection. Here, the matching of the two layers is realised by U_*^x, which accounts for the modification of the friction at the surface in connection with the differential gravity forces acting between the wall and the free-stream bubble layers. The gravity effect is even more obvious when introducing the frictional Froude number, F_{R*}, in [5]. That is,

$$U_*^{x2} = \beta^2 U_*'^2 \quad \text{where} \quad \beta^2 = \left(1 - \frac{F_{R*}\epsilon_x}{t^2}\right); \quad F_{R*} = \frac{g\overline{D_B}}{U_*'^2}; \quad t^2 = \left(\frac{U_*'}{U_*}\right)^2_{\mathrm{Re}\delta = \mathrm{cst}}; \quad \epsilon_x = \epsilon_P - \epsilon_E. \qquad [6]$$

Calculation of U_*^x from the measured values of U_*' (Moursali *et al.* 1995a) indicates that it is slightly lower than the single-phase friction velocity U_* (table 1). The problem is now the determination of the modified additive constant C^x. Keeping in mind that the sublayer thickness, s, is unchanged when scaling the profile with U_*' (section 5.1), the expression of C^x can be easily obtained as

$$C^x - C = s\left(\frac{1}{\beta} - 1\right) - \frac{1}{K}\mathrm{Ln}(\beta). \qquad [7]$$

The agreement between the value thus calculated and that deduced from the data is good (figure 9). The assumption of a constant sublayer thickness is therefore quite acceptable. The fact that U_*^x is the correct matching velocity scale for the overlapping region is yet more obvious when considering the same profiles under their defect form (U_L is replaced by $U_{Ld} = U_{LE} - U_L$, figure 10.) Indeed, all the data collapse nicely onto the same logarithmic law, as for single-phase turbulent boundary layers on a flat plate. In particular the wake strength, $2\Pi^x/K$, defined by Coles (1956) keeps it typical plate value of 2.35. The validity of the above can be checked in an ultimate way, by deriving the wall friction law associated with the modified logarithmic law, and by comparing

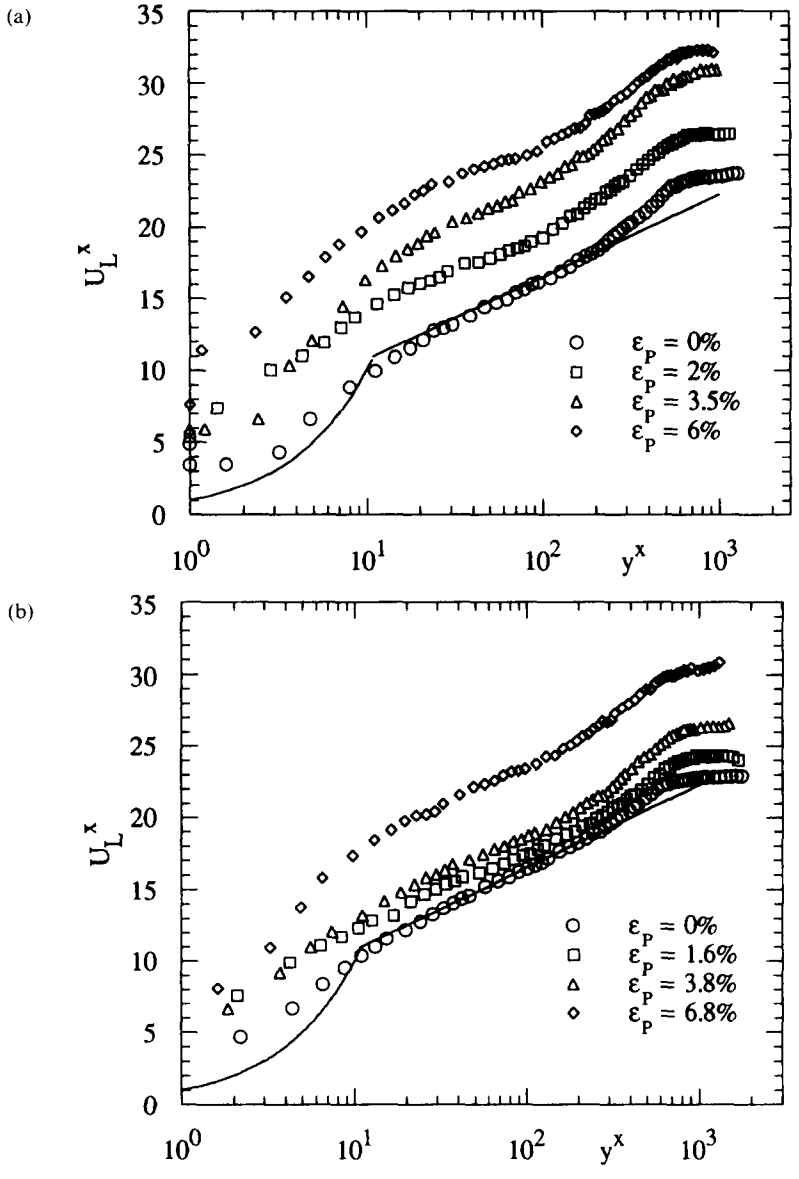

Figure 7. Velocity profiles replotted using the velocity scale defined by [5]. $x = 1$ m. — theory ($\varepsilon_P = 0\%$). Log law: $2.5 \ln y^+ + 5$. (a) $U_{LE} = 0.75$ m/s, (b) $U_{LE} = 1$ m/s.

the measurements recently published (Moursali *et al.* 1995a). The two laws of friction without and with bubbles are written, respectively, as

$$\frac{U_E}{U_*} = \frac{1}{K}\ln(\delta^+) + C + \frac{2\Pi}{K} \qquad [8]$$

$$\frac{U_{LE}}{U_*^x} = \frac{1}{K}\ln(\delta^x) + C^x + \frac{2\Pi^x}{K}. \qquad [9]$$

The present experiment was performed keeping the free-stream velocity constant, that is, $U_{LE} = U_E$. Moreover, the boundary layer thickness, δ, is unaffected and no modification of the wake is observed ($\Pi^x = \Pi$). Combining [8] and [9] and eliminating δ yields the final relationship

$$\frac{K}{\sqrt{t^2 - F_{R^*}\epsilon_x}}(f_0 - st) - K(f_0 - s) - \ln(t) = 0 \qquad [10]$$

in which $f_0 = \sqrt{2/C_F}$ is a function of the friction coefficient, C_F, in the single-phase boundary layer. Since ϵ_E remains low ($< 10\%$), the logarithmic term in [10] can be neglected. Subsequently, the increase of wall shear stress is the solution of a quadratic equation

$$\left(\sqrt{\frac{\tau_w}{\tau_{w0}}}\right)_{Re\delta = cst} = \frac{f_0 s - (f_0 - s)\sqrt{f_0(f_0 - (2s - f_0)F_R \cdot \epsilon_x)}}{f_0(2s - f_0)}. \qquad [11]$$

As shown in figure 11, [11] fits satisfactorily the trends exhibited by the data. In particular, the fact that the wall shear stress increases with ϵ_x and that, for constant ϵ_x, the increase is greater for low values of the external velocity is well reproduced. We conclude that over the range of flow conditions investigated, the dominant mechanism involved in the flattening of the velocity profile, and therefore in the increase of the wall gradient, is the gravity effect created by the high concentration bubble layer close to the surface. Also, we see on the same figure that the previous model proposed by Marié (1987a) greatly underestimates the action of the gas, especially at low

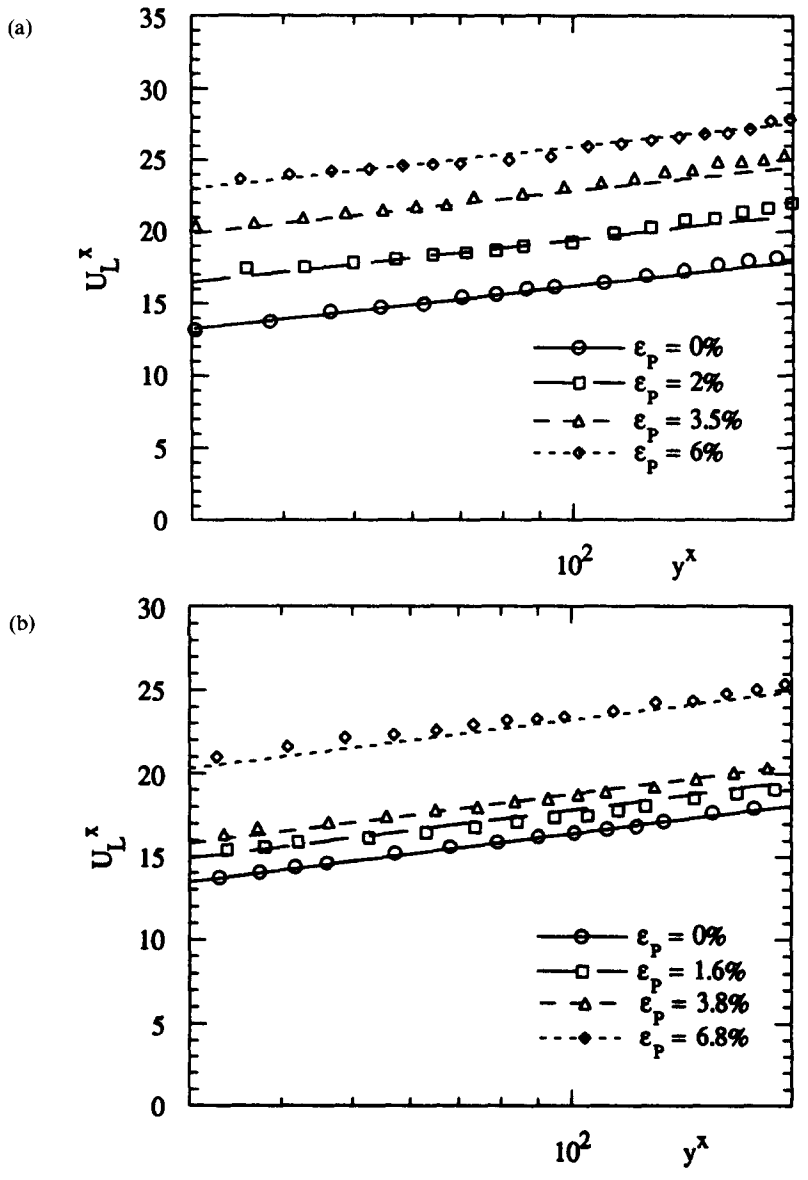

Figure 8. Enlarged view of the logarithmic profiles. $x = 1$ m. — Log law: $2.5 \ln y^+ + 5$. Other lines: interpolation. (a) $U_{LE} = 0.75$ m/s, (b) $U_{LE} = 1$ m/s.

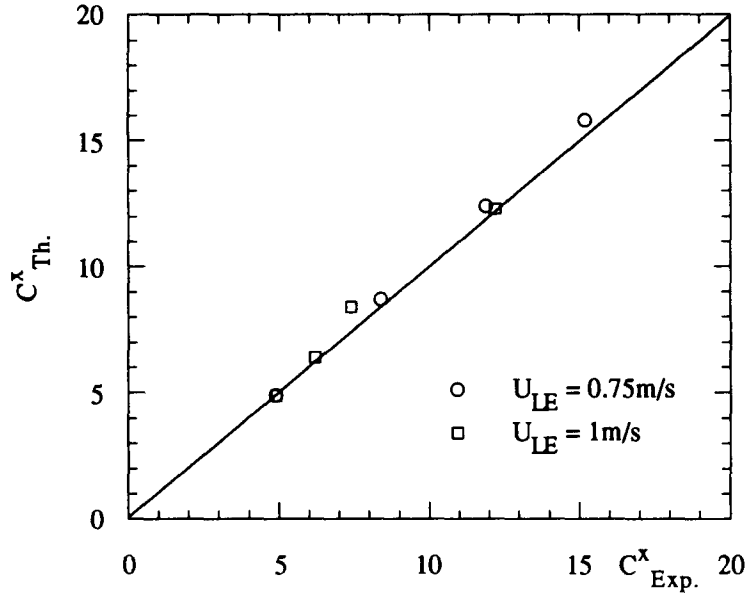

Figure 9. Additive constant in the logarithmic velocity profiles: [7] and experiment.

external velocity. This is not surprising in so far as this model assumes that the flattening results from the pseudo-turbulence generated by the bubbles in the outer layer. In the current work, since the free-stream void fraction, ϵ_E, is particularly low ($<1.5\%$), this complementary mechanism is masked by the mechanism described above. A similar trend has been found with the fluid entrainment process in gravity driven bubble flows (Mareuge and Lance 1995).

4.3. *Comparison with bubbly flows in pipes*

Bubbly flows in vertical pipes have been studied extensively in a number of experiments. Unfortunately, most of the data which are available, are not scaled in terms of wall-variables, making the comparison with our results impossible. To our knowledge, the only exception since the pioneering approach of Sato *et al.* (1981), is the recent work presented by Nakoryakov and Kashinsky (1995). It concerns two distinct situations.

The first one, investigated in the past (Nakoryakov *et al.* 1981), is an upflow in a 86.4 mm diameter pipe, with superficial liquid velocities up to 1.06 m/s, and volumetric air qualities up to 0.18. The mean size of the bubbles is of the order of 2–3 mm and the resulting void fraction profiles are of the wall-peaking type. The measurements which were performed using an electrochemical method, show in this case that the modifications of the velocity profiles are similar to those exhibited in figures 5 and 6. The logarithmic law is seen to persist in the range $5\% < \epsilon_E < 10\%$–$10\% < \epsilon_P < 30\%$, with a slope which decreases more or less, depending on the magnitude of $\epsilon_x = \epsilon_P - \epsilon_E$. This supports the idea that the mechanisms are the same as for the plate and that the present modelling should apply. If we transpose the scaling analysis of section 4.2 to pipe flows, we find that the equations are basically unchanged. The difference lies simply in the fact that Π, C_f in [8]–[11] are replaced by their expression for pipes and δ by the radius R. The law of the wall thus obtained holds under the assumptions already stated (the velocity at the centre of the pipe is kept constant, and the void fraction in the core is low $\epsilon_E < 1.5\%$). Its validity has not yet been checked against the data of Nakoryakov and Kashinsky. A priori we can expect a good agreement if the gravity forces are predominant for their flow conditions. Otherwise it is probable that the law has to be corrected to account for additional effects (see last paragraph).

The second situation is a downflow in a 42.3 mm diameter pipe, with superficial liquid velocities up to 1 m/s and volumetric air qualities up to 0.15. The bubble diameter is of order of 1.5 mm, but contrary to the previous case, a typical void-coring distribution is generated.

Measurements indicate that the velocity profiles are flattened, though there is no gas at the wall. This means that the flattening is produced by the effect of the bubbles in the external part of the boundary layer. As in upflow, the persistence of the logarithmic law is observed for ϵ_E up to 11%. However, the trends are inverted: the Von Karman constant is found to be unchanged when the profiles are scaled with U_* (figure 12(a)), while the wake function $2\Pi^x/K$ is depressed significantly depending on ϵ_E. Such modifications are particularly visible in figure 12(b), where the data have been replotted by the present authors in the corresponding defect form. They were already noted by Marié (1987a) in his analysis of the measurements of Sato *et al.* (1981) and were modelled as being caused by the bubble-induced turbulence (the acceleration of the liquid in the core was neglected). The remarkable thing is that [7], [9] and [10] remain valid for such a void distribution, provided that $\epsilon_x = 0$ or $\epsilon_* = \epsilon_E$. The latter condition can be considered as the correct approximation for incorporating the coring-effect in our model. Taking $\epsilon_* < \epsilon_E$ would have no sense, since it does not yield the right logarithmic

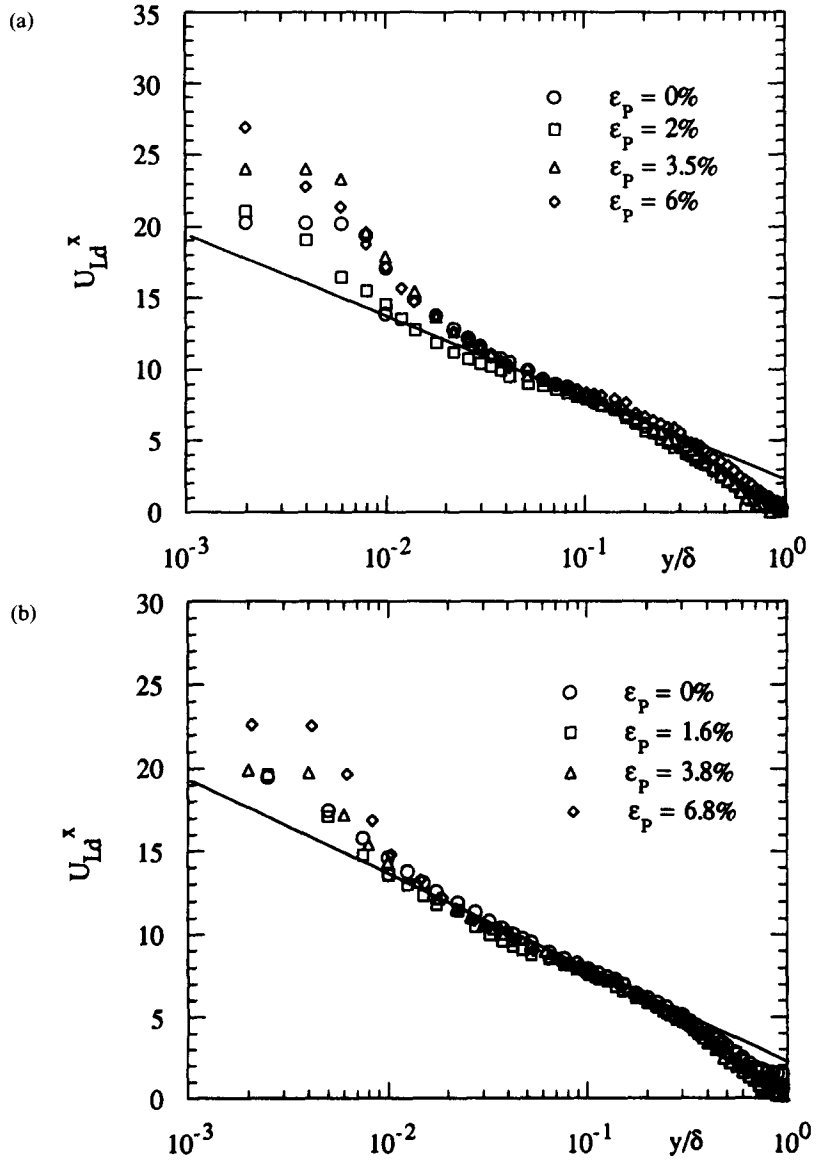

Figure 10. Defect velocity profiles plotted using the velocity scale defined by [5]. $x = 1$ m. — Log law: $-2.5 \ln (y/\delta) + 2.35$. (a) $U_{LE} = 0.75$ m/s, (b) $U_{LE} = 1$ m/s.

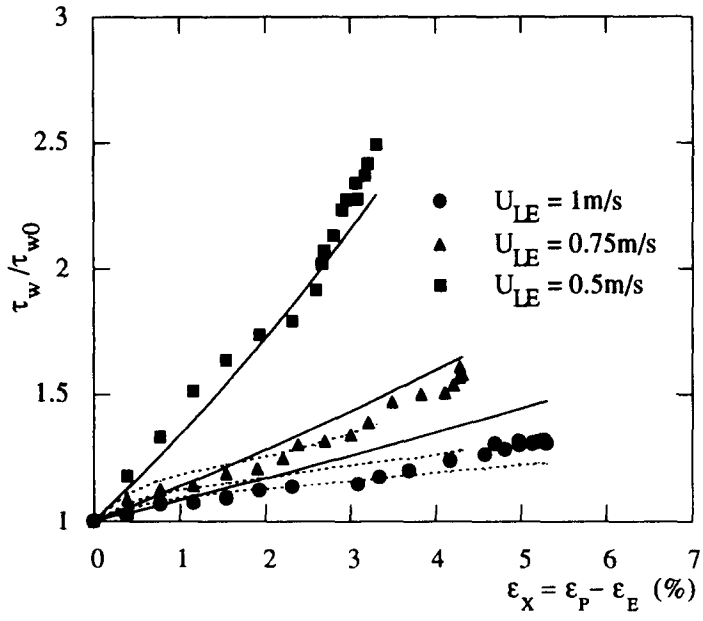

Figure 11. Wall shear stress increase. - - - [32] in Marié (1987a); — [11] present modelling.

scaling and wall shear stress (a decrease is obtained in place of an increase). For constant free-stream velocity, the law of friction then becomes

$$Kf_0\left(\frac{1}{t}-1\right)-\ln(t)-2(\Pi^x-\Pi)=0 \qquad [12]$$

in which the wake shift, $\Pi^x - \Pi$, is the only quantity to be determined. It can be expressed using [20] of the reference above.

At this level, it seems therefore difficult to derive a general expression for the law of the wall in bubbly flows. The reason is that it depends strongly on the void fraction distribution, itself a function of the size, the granulometry of the bubbles, the flow direction (upward, downward or horizontal) and to some extent, on the geometry. The difficulty was mentioned by Lopez de Bertodano (1995) in his attempt to obtain such a law, and is particularly obvious for the modification of the wall shear stress, where various tendencies are observed, according to the bubble size spectrum (Liu *et al.* 1993; Marié 1987b). However, combining the two complementary cases associated with [10] and [12], provides a generalization of the initial approach, in which both the effects of the wall-peak and of the bubbles in the core (bubble-induced turbulence plus acceleration U_{LE}/U_E) are included. The resulting law of friction is written as

$$\frac{K}{\sqrt{t^2-F_{R*}\epsilon_x}}\left(f_0\frac{U_{LE}}{U_E}-st\right)-K(f_0-s)-\ln(t)-2(\Pi^x-\Pi)=0. \qquad [13]$$

In this form, the law is likely to work for the void-peaking and void-coring situations reported here. Of course, this has to be confirmed by a quantitative comparison with the data. One point is clear, [13] remains limited to the range where the logarithmic law persists. For downflow (figure 12(b)) such a persistence tends to vanish as ϵ_E increases above 10%, probably due to the complexity and the diversity of processes involved (confinement effects, bubble interaction, other characteristic scales . . .). Thus, we may expect for ϵ_E an upper limit of the order of 15%, and the same in upflow. In terms of bubble diameter, the modelling should be physically relevant for bubbles with a mean diameter say, between 1 and 6 mm. A more precise estimation is difficult. Over that range, we must keep in mind that the critical size for the transition between void-peaking and void-coring varies with the diameter of the pipe (Kashinsky *et al.* 1995), in a way which has still to be elucidated.

As in single-phase flows, the nature of the wall surface (smooth or with roughness) is another parameter to be examined (see for example Takamasa and Kondo 1995, for the influence on the void distribution). Intuitively, the existence of a roughness k should not invalidate the choice of the matching velocity U_*^* (U_*' for the void-coring), but should produce its standard effect on the additive constant C, function of the ratio $\hat{k}U_*/\nu$.

Eventually, it is useful to derive the relationship between K and K', the modified Von Karman constant, in figure 6. Simple substitution between [8] and [9] provides

$$K' = \frac{K}{\sqrt{1 - \frac{F_{R^*}\epsilon_x}{t^2}}} \qquad [14]$$

where t is determined by [11].

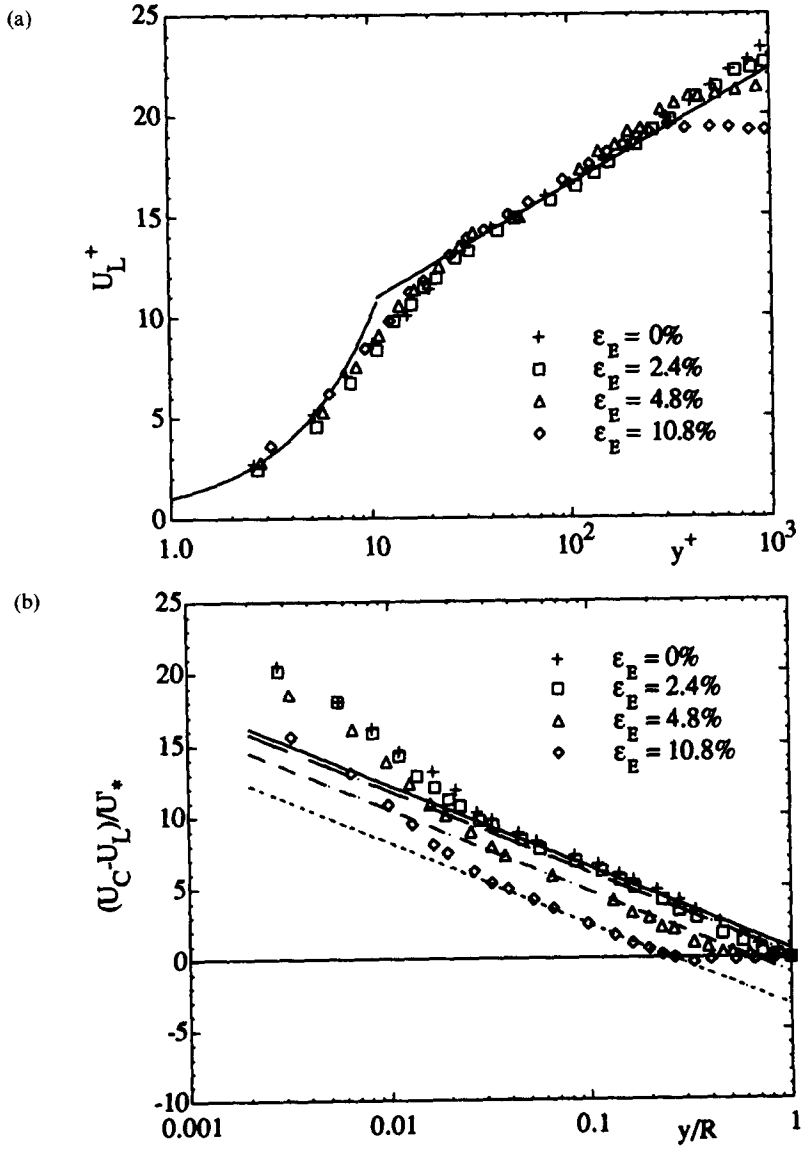

Figure 12. (a) Data of Nakoryakov *et al.* (1995) for downward bubbly pipe flows (D_B = 1.5 mm), plotted using the two-phase friction velocity U_*'; Log law: 2.5 ln y^+ + 5. (b) The same data replotted by the present authors under the corresponding non-dimensional defect form. Single-phase log law (+): $-2.5 \ln (y/R) + 0.65$.

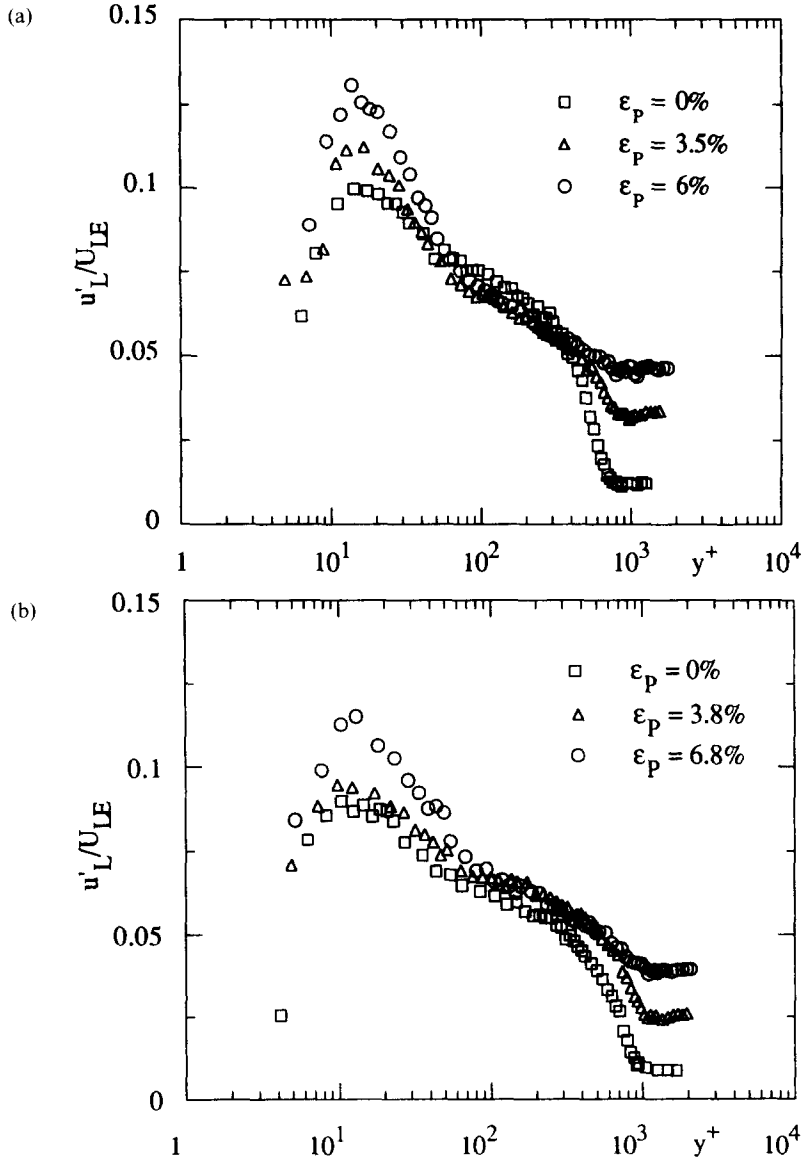

Figure 13. (a) Longitudinal turbulent intensity profiles at station $x = 1$ m. (a) $U_{LE} = 0.75$ m/s. (b) $U_{LE} = 1$ m/s.

5. SOME TURBULENT CHARACTERISTICS

5.1. *Longitudinal turbulence intensity profiles*

As shown in figure 13, the longitudinal turbulence intensity increases significantly in the presence of the bubbles. Such an increase is not systematic in pipe flows where, depending on the flow conditions, a decrease in the turbulence is sometimes observed (Serizawa *et al.* 1975; Wang *et al.* 1987). Here, three distinct zones are observed on the profiles. In the free-stream and outer region ($Y^+ > 800$), the increase in the turbulent kinetic energy, $u_L'^2$, compared with its single-phase value, $u_{L0}'^2$, is found to be proportional to $\epsilon_E U_R^2$ (figure 14), suggesting that the pseudo-turbulence generated by the bubbles is the dominant effect (Lance and Bataille 1991). The proportionally factor is 1.4, which is slightly greater than the upper limit calculated with the potential theory of Lance and Bataille (1991). This difference may be connected to some extra production in the bubble wakes. Close to the wall ($Y^+ = 10$–30), the higher intensity proves to be proportional to the two-phase friction velocity U_*' (figure 15), which implies that the mechanism prevailing in that zone is an enhancement of the wall production caused by the higher velocity gradient (see section 4).

As can be noticed, the location of the maximum of the wall production remains unchanged. Surprisingly, no significant modification occurs in the intermediate region ($30 < Y^+ < 200$), where the void fraction is maximum. In fact, measurements indicate that in this layer, the velocity of the bubbles at $y \approx \bar{D}_B/2$, is on average only slightly different from that of the liquid (Moursali *et al.* 1995a), meaning that the pseudo-turbulence effects are necessarily weak. Under such conditions, the remaining mechanism is the increase of the wall production by the bubbles. The fact that the turbulence level is not modified supports the idea that the dissipation process adapts itself to this extra-energy, or in other words, that the equilibrium production-dissipation is conserved. This is consistent with the existence of a logarithmic region and [5]. Indeed, according to the latter, $-\overline{u_L v_L}^x \approx U_*^2$ in this overlapping area, and since U_* is on average lower than U_* we deduce that $\overline{u_L^2}^x \approx -\overline{u_L v_L}^x$ should decrease or at least remain constant over this area.

The two mechanisms of turbulence production which have been identified, prove to be statistically independent. This holds in the limited range of flow conditions which has been

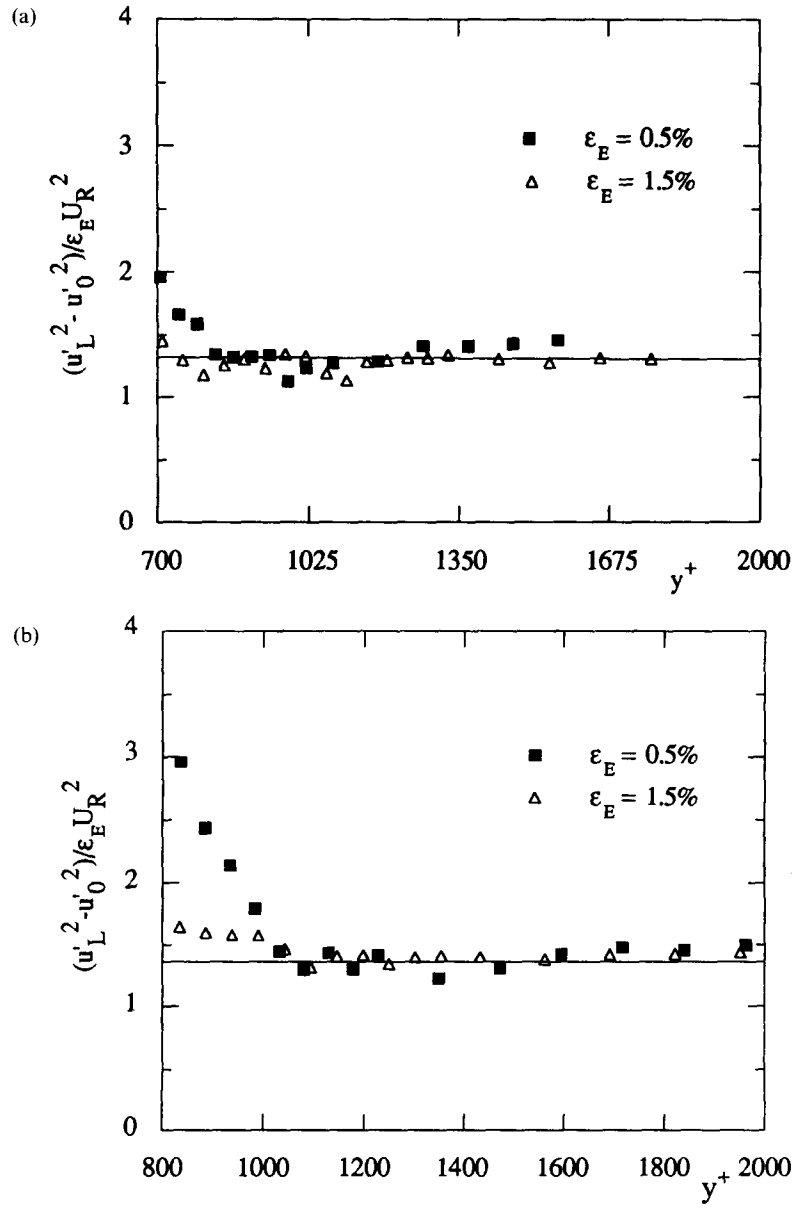

Figure 14. Outer region: excess longitudinal turbulent kinetic energy scaled by $\epsilon_E U_R^2$. $x = 1$ m. $U_{LE} = 0.75$ m/s, (b) $U_{LE} = 1$ m/s.

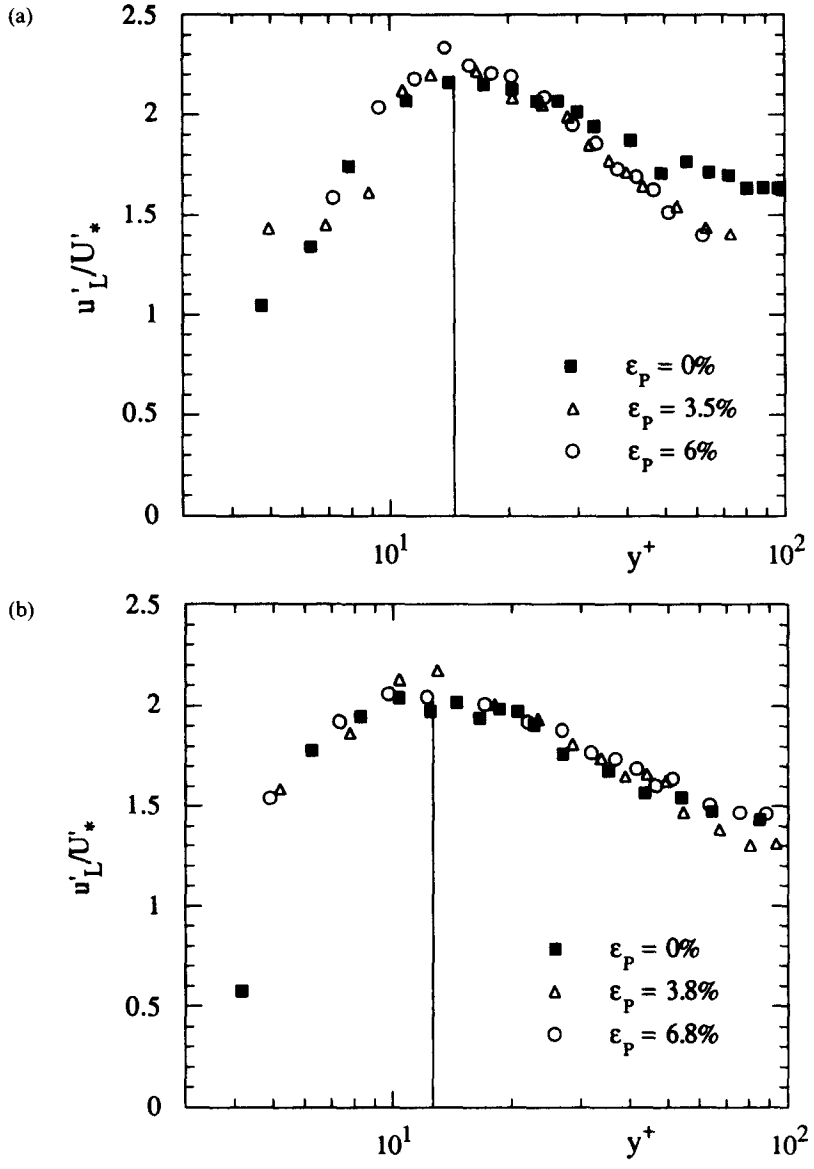

Figure 15. The longitudinal wall production scaled by U'_*. $x = 1$ m. (a) $U_{LE} = 0.75$ m/s, (b) $U_{LE} = 1$ m/s.

investigated. Obviously, when the void fraction in the outer layer is much greater, there is no serious reason for thinking that the same situation will persist. In such a case, the two processes will probably interact and compete with each other. In view of these findings, we now understand that a local decrease of the turbulence in the outer layer of the flow, may directly result from the flattening of the velocity shape in that region, leading to a decrease of the shear induced turbulence. If this decrease is larger than the increase associated with the pseudo-turbulence, then a global decrease of the turbulence level can be expected. This is the trend which appears in the logarithmic region of figure 13(a). However, the decrease is so small that it could be interpreted as the result of some measurement uncertainty. Nonetheless, it is more likely to have a physical meaning since it occurs for $U_{LE} = 0.75$ m/s—that is for flow conditions where the flattening is particularly pronounced (figure 5) compared with the case $U_{LE} = 1$ m/s.

5.2. Mixing length

From the previous sections, it follows that the concept of a mixing length is still valid for describing turbulent bubbly boundary layers in which the logarithmic law is preserved. Provided

that an adequate matching velocity, U_*^*, is chosen, the mixing length, l_x, in the overlapping region keeps the standard single-phase proportionality to the distance from the wall ($l_x = KY$). However, using U_* in place of U_*^*, as in single-phase flows, yields for the mixing length another expression, l', of the form $K'Y$, where K' can be considered as a modified Von Karman constant and deduced from [11]–[14].

In some experiments as for example in Serizawa *et al.* (1975), a mixing length, l_u, is inferred from the longitudinal turbulent intensity and mean velocity profiles as

$$l_u = u'_L \left(\frac{dU_L}{dY} \right)^{-1}. \qquad [15]$$

As shown in figure 16,, the variation of l_u calculated from our two-phase flow data is roughly linear, but given the significant scattering this cannot be considered as additional evidence of the persistence of the logarithmic law.

Finally, it is worthwhile noting that the values of l' inferred from the measurements prove to be in reasonable agreement (figure 16) with that derived by Kataoka and Serizawa (1991), and Sato and Sekoguchi (1975), using two different turbulence models. This is not the case for the model of Rice and Geary (1990) for bubble columns, which greatly overestimates the mixing length at the surface.

6. CONCLUSION

The first noticeable and quite unexpected result is the persistence of the single-phase flow structure. In particular it is found that an overlapping logarithmic region still exists close to the plate. However, the adequate velocity scale for describing that region is not the friction velocity as in single-phase boundary layers, but a velocity scale which accounts for the gravity effects caused at the surface by the peak of void fraction. The kinematic structure is thus unaffected whereas the local momentum transfer is significantly modified. The same qualitative behaviour has been reported for other types of bubbly shear flow such as a plane mixing layer or a sudden expansion (Lance *et al.* 1995). It must be kept in mind that these conclusions are restricted to the limited range of void fraction investigated and it would be dangerous to extrapolate them to flows with higher void fractions.

Concerning the effect on the turbulence, the mechanisms which have been identified are those involved in most of bubbly flows, that is the modification of the shear induced turbulence and the

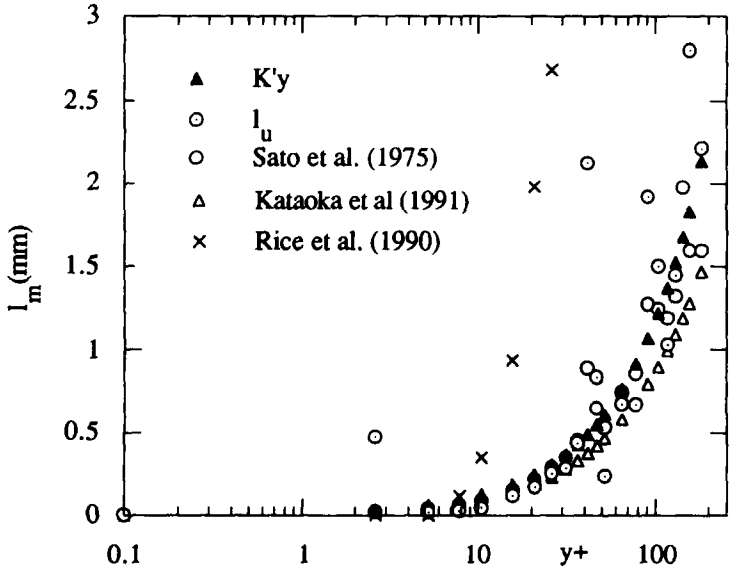

Figure 16. The mixing lengths in the wall region at station $x = 1$ m; $U_{LE} = 1$ m/s; $\epsilon_P = 7\%$.

creation of pseudo-turbulence associated with the drift motion and the wake of the bubbles. These two basic contributions (which linearly superpose in the limit of vanishing void fraction in uniform bubbly flows (Lance and Bataille 1991) or in weak shear flows (Lance *et al.* 1991)) are well distinguished here. The first is predominant close to the wall whereas the second one prevails in the outer layer. However, it is expected that the two will interact at higher void fractions through complex non-linear phenomena. The investigation of this range of flow conditions would be particularly interesting and is our future objective.

Acknowledgements—The present work was partially funded by the Direction des Recherches, Etudes et Techniques, Centre National de la Recherche Scientifique (Gredic), Ministère de la Recherche et de L'Education Nationale (Alliance Program).

Special thanks are expressed by Dr J. L. Marié and E. Moursali to Professor M. Lance for the very efficient role he played in finding the extra financial support to complete the present part of the research programme.

The authors express their gratitude to Dr A. J. White for supervising the English.

REFERENCES

Cartellier, A. and Achard, J. L. (1985) Limitations of the classical LDA formula for velocity measurements for large particles in two-phase suspension flows. *PCH J.* **6,** 463–481.

Coles, D. (1956) The law of the wake in the turbulent boundary layer. *J. Fluid Mech.* **1,** 191–226.

Hancock, P. E. and Bradshaw, P. (1983) The effect of free-stream turbulence on turbulent boundary layers. *ASME J. Fluids Engng* **105,** 284–289.

Ishii, M. (1975) Thermo-fluid dynamic theory of two-phase flow. Collection Etudes et Recherches EDF, Eyrolles.

Kashinsky, O. N., Gorelik, R. S. and Randin, V. V. (1995) Upward bubbly flow in small-diameter vertical pipe. *Russ. J. Eng. Thermophys.* **5,** 177–193.

Kataoka, I. and Serizawa, A. (1991) Bubble dispersion coefficients and turbulence diffusivity in bubbly two-phase flow. *ASME Turbulence Modification in Multiphase Flows*, Vol. 110, pp. 59–66, Portland, Oregon.

Klebanoff, P. S. (1955) Characteristics of turbulence in a boundary layer with zero pressure gradient. Naca report. 1247.

Lance, M. and Bataille, J. (1991) Turbulence in the liquid phase of a uniform bubbly air–water flow. *J. Fluid Mech.* **222,** 95–118.

Lance, M., Marié, J. L., Moursali, E. and Bataille, J. (1991) Homogeneous turbulence in bubbly flows. *ASME J. Fluids Engng* **113,** 295–300.

Lance, M. and Lopez de Bertodano, M. (1992) Phase distribution phenomena and wall effects in bubbly two-phase flows. Presented at the *3rd International Workshop on Two-phase Flow Fundamentals*, Imperial College, London.

Lance, M., Marié, J. L., Moursali, E., Bataille, J., Suzanne, C., Roig, V., Bel F, Dhila, R. and Masbernat, L. (1996) Experimental study of turbulent bubbly shear flows. *Chem. Engng Comm.* **141–142,** 51–70.

Liu, T. J. (1993) Bubble size and entrance length effects on void development in a vertical channel. *Int. J. Multiphase Flow* **19,** 99–113.

Liu, T. J., Hong, W. T. and Yeh, F. Z. (1993) Wall shear stress and its fluctuations in vertical bubbly flow under different initial bubble size conditions. *29th Nat. Heat Transfer Conf*, Atlanta.

Lopez de Bertodano, M. (1995) Development of a two-phase law of the wall for bubbly flows. Presented at the *2nd International Conference on Multiphase Flow '95*, Vol. 4, PI23–PI30, Kyoto.

Mareuge, I. and Lance, M. (1995) Bubble induced dispersion of a passive scalar in bubbly flows. Presented at the *2nd International Conference on Multiphase Flow '95*, Vol. 2, PTI3–PTI8, Kyoto.

Marié, J. L. and Lance, M. (1983) Turbulence measurements in two-phase bubbly flows using laser doppler anemometry. *IUTAM Symposium*, Nancy, pp. 141–148. Springer, Berlin.

Marié, J. L. (1983) Investigation of two-phase bubbly flows using laser doppler anemometry. *PCH J.* **4,** 103–118.

Marié, J. L. (1987a) Modelling of the skin friction and heat transfer in turbulent two-component bubbly flows in pipes. *Int. J. Multiphase Flow* **13,** 309–325.

Marié, J. L. (1987b) A simple analytical formulation for microbubble drag reduction. *PCH J.* **8,** 213–220.

Monji, H. and Matsui, G. (1991) Effect of bubble size on structure of vertical bubble flow. In *Proc. of the Int. Conf. on Multiphase Flows*, pp. 449–452, Tsukuba.

Moursali, E. (1993) Etude expérimentale d'une couche limite eau-air à bulles se développant sur une plaque plane verticale. Ph.D. thesis, Lyon.

Moursali, E., Marié, J. L. and Bataille, J. (1995a) An upward turbulent bubbly boundary layer along a vertical flat plate. *Int. J. Multiphase Flow* **21,** 107–117.

Moursali, E., Marié, J. L. and Bataille, J. (1995b) Law of the wall and turbulent intensity profiles in a bubbly boundary layer at low void fractions. Presented at the *2nd International Conference on Multiphase Flow '95*, Vol. 4, PI17–PI21, Kyoto.

Nakoryakov, V. E., Kashinsky, O. N., Burdukov, A. P. and Odnoral, V. P. (1981) Local characteristics of upward gas-liquid flows. *Int. J. Multiphase Flow* **7,** 63–81.

Nakoryakov, V. E. and Kashinsky, O. N. (1995) Gas–liquid bubbly flows in a near-wall region. In *Proc. of the 1st International Symposium on Two-phase Flow Modelling and Experimentation*, pp. 453–457. Rome.

Rice, R. G. and Geary, N. W. (1990) Prediction of liquid circulation in viscous bubble columns. *AIChE J.* **36,** 1339–1348.

Sato, Y. and Sekoguchi, K. (1975) Liquid velocity distribution in two-phase bubble flow. *Int. J. Multiphase Flow* **2,** 79–95.

Sato, Y., Sadatomi, M. and Sekoguchi, K. (1981) Momentum and heat transfer in two-phase flow. Parts I and II. *Int. J. Multiphase Flow* **7,** 167–190.

Schlichting, H. (1968) *Boundary Layer Theory*, 6th Edition. McGraw-Hill, New York.

Serizawa, A., Kataoka, I. and Michiyoshi, I. (1975) Turbulence structure of air–water bubbly flow. Parts I–III. *Int. J. Multiphase Flow* **2,** 221–259.

Serizawa, A., Kataoka, I., Zun, I. and Michiyoshi, I. (1988) Bubble size effect on phase distribution. In *Proc. of the Japan–US Seminar on Two-phase Flow Dynamics*, pp. 15–20, Ohtsu, Japan.

Souhar, M. (1989) Some turbulence quantities and energy spectra in the wall region in bubble flows. *Phys. Fluids A* **1,** 1558–1565.

Takamasa, T. and Kondo, K. (1995) Effects of wall roughness on bubble motion in rectangular tube. *Two-phase Flow Modelling and Experimentation*, eds G. P. Celata and R. K. Shah, Vol. 1, pp. 361–366. ETS.

Tennekes, H. (1965) Similarity laws for turbulent boundary layers with suction or injection. *J. Fluid Mech.* **21,** 689–703.

Tennekes, H. and Lumley, J. L. (1972) *A First Course in Turbulence*, pp. 146–196. MIT Press, Cambridge, MA.

Tran-Cong, S., Marié, J. L. and Perkins, R. J. (1996) Statistical results on bubble trajectories in a turbulent boundary layer. *Advances in Turbulence VI*, eds S. Gavrilakis *et al.*, pp. 573–574. Kluwer Academic Publishers, Dordrecht.

Wang, S. K., Lee, S. J., Jones, O. C. and Lahey, R. T. (1987) 3-D turbulence structure and phase distribution measurements in bubbly two-phase flows. *Int. J. Multiphase Flow* **13,** 327–343.

Zun, I., Kljenak, I. and Serizawa, A. (1992) Bubble coalescence and transition from wall void peaking to core void peaking in turbulent bubbly flow. In *Dynamics of Two-phase Flows*, eds O. C. Jones and I. Michiyoshi, pp. 233–249. Boca Raton, FL.